Pergamon

PII: S0191-8141(98)00025-X

Journal of Structural Geology, Vol. 20, No. 8, pp. 1105 to 1120, 1998

0191-8141/98 $19.00 + 0.00

High-strain zones: a unified model

DAZHI JIANG and PAUL F. WILLIAMS

Department of Geology, University of New Brunswick, Fredericton, New Brunswick, Canada, E3B 5A3,
E-mail: zjiang@unb.ca

(*Received* 9 *December* 1997; *accepted in revised form* 4 *March* 1998)

Abstract—Where a shear zone is bounded by undeformed wall rocks and there is no volume change, the deformation path within the zone on the bulk scale approximates a simple shear. Where the zone boundaries are stretched and the shear direction between the two boundaries is parallel to one of the principal stretching directions of the boundaries, the deformation path within the zone is not a simple shear but still has monoclinic symmetry. Both simple shear and general monoclinic deformation paths should be regarded as special cases in nature, because generally not only are the zone boundaries stretched but also the shear is oblique to the principal stretching directions of the boundaries. In this general case, the deformation path is triclinic. We establish a model which includes this general case also taking into consideration volume change.

Five independent parameters are required to characterize the rate of deformation of the flow; four are sufficient to characterize the flow kinematics. The model is generally triclinic, and orthorhombic and monoclinic deformations are subgroups. By varying the values of the characterizing parameters, the various types of high-strain zones can be represented. The kinematics of flow within such zones and the accumulated finite deformation geometry are investigated. Many field observations such as, for example, lineations in transcurrent shear zones that vary between vertical and horizontal, cleavage transected folds, and the absence of sheath folds in some shear zones where folds have been significantly rotated, can sometimes be better interpreted in the context of our general model. © 1998 Elsevier Science Ltd. All rights reserved

INTRODUCTION

Localization of strain into high-strain zones is a common feature of natural deformation. In early plane-strain models, these zones were called shear zones (Ramsay and Graham, 1970; Ramsay, 1980) or ductile deformation zones (Mitra, 1978). Sanderson and Marchini (1984) used the term transpression (transtension) to refer to their three-dimensional model. Subsequent authors (see below) adopt this term when they revise or expand the model of Sanderson and Marchini (1984). However, as pointed out by Robin and Cruden (1994), the term transpression has a dual meaning of both tectonic environment (Harland, 1971) and deformation path which must be clearly distinguished in the study of natural deformation (Lister and Williams, 1979; Williams and Schoneveld, 1981; Celma, 1982; Platt and Behrmann, 1986; Robin and Cruden, 1994; Jiang, 1994a; Jiang and White, 1995). Because of this and because this paper deals with a general model in which existing models become special cases, the term 'high-strain zone' is used to refer to all natural zones of strain concentration.

Ramsay and Graham (1970) and Ramsay (1980), following a finite deformation approach, demonstrated that the deformation path within a zone of constant volume, bounded by undeformed wall rocks, approximates a simple shear on the bulk scale. Ramberg (1975) presented an elegant analysis of all two-dimensional, isochoric, homogeneous, steady deformations in terms of rate of deformation. Ramberg's work is now classic and the method can be extended to three-dimensional deformations. By considering the velocity field as a function of time and position, the method can also deal with heterogeneous and non-steady deformations. Following a finite deformation approach, Sanderson and Marchini (1984) proposed the first three-dimensional model for high-strain zones which they called transpressional zones. Other models have been published in many papers including Jones and Tanner (1995), Krantz (1995) and Teyssier *et al.* (1995). Fossen and Tikoff (1993) and Tikoff and Teyssier (1994) formulated Sanderson and Marchini's model in terms of rate of deformation following Ramberg's approach. Robin and Cruden (1994) investigated the flow geometry of an extrusional high-strain zone model where the boundary-normal component of the relative velocity of the zone is accommodated in the same volume of rock as the boundary-parallel component of the relative velocity. The finite strain geometry of this model has been investigated by Dutton (1997). Jones *et al.* (1997) extend the Sanderson and Marchini (1984) model to include all three-dimensional monoclinic and constant-volume deformations.

A simple shear path is monoclinic. The deformation path in a high-strain zone with stretching boundaries and with shear direction (boundary-parallel component of the relative velocity of a high-strain zone, see below) parallel to one of the principal stretching directions of the boundaries is also monoclinic. It is obvious that such monoclinic situations are special cases. Once the shear direction is oblique to the principal stretching directions of the boundaries, the

high-strain zone becomes triclinic (Robin and Cruden, 1994; Lin *et al.*, 1998). As will be discussed later in the paper, such boundary conditions are very common in nature from the scale of plate boundaries to a single deformation zone. Natural high-strain zones that cannot be properly interpreted in terms of a monoclinic deformation path are reported for example from the Canadian Appalachians (e.g. Caron and Williams, 1988; Lin, 1992; Goodwin and Williams, 1996; Lin *et al.*, 1998) and Sveconorwegian orogenic province of southwest Sweden (Robin and Cruden, 1994).

We present a general model for high-strain zones expanding the work of Lin *et al.* (1998) to include biaxial stretching of the boundaries and volume change. Monoclinic models are not excluded but form a subgroup. In fact, by varying the characterizing parameters, the deformation path of our model varies from coaxial through monoclinic non-coaxial (including simple shear) to general triclinic non-coaxial.

CHARACTERIZATION OF FLOW

Figure 1 shows a homogeneous domain of a high-strain zone. In the most general situation (Fig. 1b), the flow can be characterized by the following five parameters. The boundaries are being biaxially stretched with two principal stretchings $\dot{\epsilon}_a$ and $\dot{\epsilon}_c$ ($|\dot{\epsilon}_a| \leq |\dot{\epsilon}_c|$ by definition). The stretching normal to the zone boundary is denoted by $\dot{\epsilon}_b$. The high-strain zone is said to be *thinning*, *thickening* or of *constant-thickness* if its two material boundaries are moving toward each other ($\dot{\epsilon}_b < 0$), away from each other ($\dot{\epsilon}_b > 0$) or maintaining the same spacing ($\dot{\epsilon}_b = 0$), respectively. The terms are chosen to distinguish these zones from the widening and narrowing zones of Means (1995) where the zone boundaries migrate through the material. The shearing (shear strain rate) on the boundary is $\dot{\gamma}$; the shear direction makes an angle ϕ with the $\dot{\epsilon}_a$ direction.

These five parameters completely characterize the flow at an instant. In order to relate them to the relative velocity of a high-strain zone, we use a reference frame, $x_1x_2x_3$, fixed to one boundary, such that x_1, x_2 and x_3 are parallel to $\dot{\epsilon}_a$, $\dot{\epsilon}_b$ and $\dot{\epsilon}_c$, respectively, and they form a right-hand coordinate system (Fig. 1b).

In such a coordinate system, the relative velocity vector, $\mathbf{v}$, of the zone (the velocity of one boundary with respect to the other) can be expressed as:

$$\mathbf{v} = v_1\mathbf{i} + v_2\mathbf{j} + v_3\mathbf{k}, \tag{1}$$

where $\mathbf{i}$, $\mathbf{j}$ and $\mathbf{k}$ are unit vectors parallel to x_1, x_2 and x_3, respectively.

The gradient of the relative velocity across the zone, i.e. along x_2 is:

$$\frac{\partial \mathbf{v}}{\partial x_2} = \frac{\partial v_1}{\partial x_2}\mathbf{i} + \frac{\partial v_2}{\partial x_2}\mathbf{j} + \frac{\partial v_3}{\partial x_2}\mathbf{k} = \frac{\partial v_{/\!/}}{\partial x_2}\mathbf{e} + \frac{\partial v_\perp}{\partial x_2}\mathbf{j}$$

$$= \frac{\partial v}{\partial x_2}(\sin\Theta\mathbf{e} + \cos\Theta\mathbf{j}), \tag{2}$$

where Θ is the angle between $\mathbf{v}$ and the zone boundary normal (x_2), $\mathbf{v}_{/\!/}$ and $\mathbf{v}_\perp$ are, respectively, the boundary-parallel and boundary-normal components of velocity ($\mathbf{v}_{/\!/} = v_1\mathbf{i} + v_3\mathbf{k}$ and $\mathbf{v}_\perp = v_2\mathbf{j}$), $\mathbf{e}$ is the unit vector parallel to $\mathbf{v}_{/\!/}$ and parallel to the shear direction (Fig. 1b). Using ϕ, we have $\mathbf{e} = \cos\phi\ \mathbf{i} + \sin\phi\ \mathbf{k}$. The magnitudes of $\mathbf{v}_{/\!/}$ and $\mathbf{v}_\perp$ are, respectively, $v_{/\!/} = v \sin\Theta$ and $v_\perp = v_2 = v\cos\Theta$.

Since $\partial v_{/\!/}/\partial x_2$ is the shear strain rate ($\dot{\gamma}$), and $\partial v_\perp/\partial x_2$ is the stretching parallel to x_2, ($\dot{\epsilon}_b$), (2) can be rewritten as:

$$\frac{\partial \mathbf{v}}{\partial x_2} = \dot{\gamma}(\cos\phi\mathbf{i} + \sin\phi\mathbf{k}) + \dot{\epsilon}_b\mathbf{j}, \tag{3}$$

and

$$\dot{\gamma} = \frac{\partial v}{\partial x_2}\sin\Theta, \quad \dot{\epsilon}_b = \frac{\partial v}{\partial x_2}\cos\Theta. \tag{4}$$

Therefore the ratio of the simple shear component to the pure shear component of the flow, $\dot{\gamma}/\dot{\epsilon}_b$, can be represented simply by $\tan\Theta$.

The model characterized above is general. The deformation path ranges from being orthorhombic to monoclinic to triclinic. Existing models of high-strain zones become subgroups of this general model:

$\dot{\gamma} = 0$ (or equivalently $\Theta = 0^\circ$), coaxial deformation path (orthorhombic or higher);

$\Theta = 90^\circ$, $\dot{\gamma} \neq 0$ and $\dot{\epsilon}_a = \dot{\epsilon}_c = 0$, Ramsay and Graham (1970) shear zone, simple shear path (monoclinic);

$0^\circ < \Theta < 90^\circ$, $\dot{\epsilon}_c = 0$, $\dot{\epsilon}_a = -\dot{\epsilon}_b > 0$ and $\phi = 0^\circ$, Ramberg (1975) plane-strain sub-simple shear (Simpson and De Paor, 1993);

$0^\circ < \Theta < 90^\circ$, $\dot{\epsilon}_a = 0$, $\dot{\epsilon}_c = -\dot{\epsilon}_b > 0$ and $\phi = 0^\circ$, Sanderson and Marchini (1984) transpression zone (monoclinic);

$\phi = 0^\circ$ and $\dot{\epsilon}_a + \dot{\epsilon}_b + \dot{\epsilon}_c = 0$ (constant volume deformation), Jones *et al.* (1997) transpression (orthorhombic or monoclinic);

$0^\circ < \Theta < 90^\circ$, $\dot{\epsilon}_a = 0$, $\dot{\epsilon}_c = -\dot{\epsilon}_b > 0$ and $0^\circ \leq \phi \leq 90^\circ$, Lin *et al.* (1998) transpression (monoclinic and triclinic);

$\dot{\epsilon}_a + \dot{\epsilon}_b + \dot{\epsilon}_c = 0$ everywhere and the characterizing parameters vary continuously across a high-strain zone and with depth, Robin and Cruden (1994) model (triclinic or monoclinic).

We wish to emphasize that the above parameters describe the flow at *an instant* in a localized body of rock. In a natural high-strain zone, these parameters vary with position and time. It is important to distinguish instantaneous and local properties from bulk (a high-strain zone as a whole) and finite properties (Lister and Williams, 1979, 1983; Williams and Schoneveld, 1981; Robin and Cruden, 1994; Jiang, 1994a,b, 1996; Jiang and White, 1995; Goodwin and Williams, 1996).

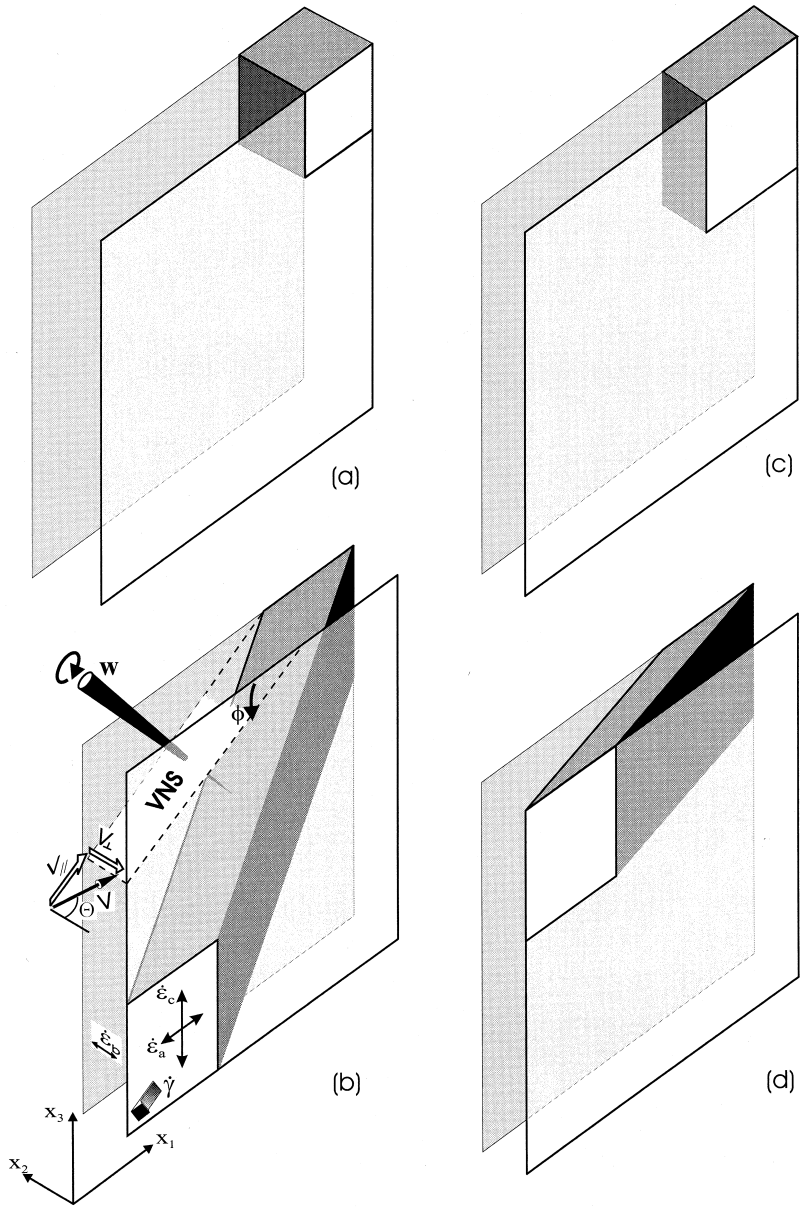

Fig. 1. A homogeneous domain in a high-strain zone showing the nomenclature used in the text. (a) The initial (undeformed) configuration. (b) The final (deformed) configuration resulting from a general triclinic non-coaxial deformation path. The velocity **V** makes an angle Θ with the zone boundary normal. It is resolved into a boundary-normal component $\mathbf{V}_\perp$, leading to thinning or thickening of the zone ($\dot{\epsilon}_b$), and a boundary-parallel component $\mathbf{V}_{/\!/}$, leading to simple shearing ($\dot{\gamma}$). The biaxial stretchings of the boundaries are $\dot{\epsilon}_a$ and $\dot{\epsilon}_c$. $x_1x_2x_3$ is the reference frame used to describe the flow. The shear direction makes an angle ϕ with respect to $\dot{\epsilon}_a$ or X_1. **W** stands for vorticity and VNS for vorticity-normal section. (c) The final configuration resulting from an orthorhombic (coaxial) path. (d) The final configuration resulting from a monoclinic non-coaxial path ($\phi = 0$). Other monoclinic situations (not shown) are $\phi = 90^\circ$ and $\dot{\epsilon}_a = \dot{\epsilon}_c$. See text for details.

FLOW KINEMATICS IN A HIGH-STRAIN ZONE

The flow within the zone is the sum of the simple shear component induced by $\mathbf{v}_{/\!/}$ and the pure shear component induced by $\mathbf{v}_\perp$. The velocity gradient tensor, **L**, in the reference frame shown in Fig. 1, can be written as (Ramberg, 1975; Lin *et al.*, 1998):

$$\mathbf{L} = \begin{pmatrix} \dot{\epsilon}_a & \dot{\gamma}\cos\phi & 0 \\ 0 & \dot{\epsilon}_b & 0 \\ 0 & \dot{\gamma}\sin\phi & \dot{\epsilon}_c \end{pmatrix}. \qquad (5)$$

L has triclinic symmetry (Fig. 1b) except for the following situations: when $\dot{\gamma} = 0$, it is orthorhombic (Fig. 1c); when $\phi = 0^\circ$, $\phi = 90^\circ$ or $\dot{\epsilon}_a = \dot{\epsilon}_c$, it is monoclinic (Fig. 1d shows the situation of $\phi = 0^\circ$). $\dot{\epsilon}_a = \dot{\epsilon}_c = 0$ is the special case of simple shear. $\dot{\epsilon}_a = \dot{\epsilon}_c > 0$ is a special thinning zone where the boundaries are stretched at the same rate in all directions.

We wish to point out that six parameters are needed to characterize the most general triclinic flow (Passchier, 1997, 1998). We deal with planar high-strain zone deformation where the vorticity vector is

constrained to be parallel to the zone boundaries and this reduces the number of characterizing parameters to five.

L can be decomposed into a stretching tensor **D** and a vorticity tensor **W** according to $\mathbf{D} = 1/2(\mathbf{L} + \mathbf{L}^{\mathrm{T}})$ and $\mathbf{W} = 1/2(\mathbf{L} - \mathbf{L}^{\mathrm{T}})$. The *intensity of stretching* (Truesdell and Toupin, 1960, p. 349) of the flow can be described by what is often referred to as the effective shear strain rate, Γ, in material science literature (e.g. Frost and Ashby, 1982). Γ is an invariant of **D** defined as (Ranalli, 1987):

$$\Gamma = (2D_{ij}D_{ij})^{1/2} = [2(\dot{\epsilon}_a^2 + \dot{\epsilon}_c^2 + \dot{\epsilon}_b^2 + 1/2\dot{\gamma}^2)]^{1/2}, \quad (6)$$

where the repeated subscript means summation over the values 1, 2 and 3 of that subscript.

For subsequent simpler presentation, we define two additional parameters, a and c to normalize $\dot{\epsilon}_a$ and $\dot{\epsilon}_c$ with respect to $\dot{\epsilon}_b$:

$$a = -\dot{\epsilon}_a/\dot{\epsilon}_b, \;\; c = -\dot{\epsilon}_c/\dot{\epsilon}_b. \quad (7)$$

Although $\dot{\epsilon}_a$ and $\dot{\epsilon}_c$ can have any values for all the equations presented in this paper, to save space, we only present results for situations where they are of the same sign, e.g. $\dot{\epsilon}_a \cdot \dot{\epsilon}_c \geq 0$. Physically this means that for a thinning zone ($\dot{\epsilon}_b < 0$) and a thickening zone ($\dot{\epsilon}_b > 0$) we have $0 \leq a \leq c$ and $0 \geq a \geq c$, respectively. The situations where $\dot{\epsilon}_a$ and $\dot{\epsilon}_c$ have different signs, which for a thinning zone for instance means that the boundaries are stretched in one direction but shortened in the orthogonal direction, are possible near the ends of high-strain zones, jogs and bends of the zone or near other geometrical irregularities. Kinematics and strain results for these situations can be readily calculated from equations presented in this paper, but the results are not presented here.

Using a and c and (4), (6) becomes:

$$\Gamma = [2\cos^2\Theta(a^2 + c^2 + 1 + 1/2\tan^2\Theta)]^{1/2}|E|, \quad (8)$$

where $E = \partial v/\partial x_2$. Figure 2 shows variation of Γ (normalized with respect to E) as a function of a, c and Θ. It is seen that Γ decreases as Θ increases, and increases as a or c approaches zero. The maximum Γ occurs when the velocity, **v**, is perpendicular to the boundary and either $\dot{\epsilon}_a$ or $\dot{\epsilon}_c$ is zero.

The dilation (volume change rate) of the flow is:

$$\delta = \dot{\epsilon}_a + \dot{\epsilon}_c + \dot{\epsilon}_b = \dot{\epsilon}_b(1 - a - c). \quad (9)$$

Passchier (1990, 1991) defined a kinematic dilatancy number to measure the two-dimensional area change rate on the vorticity-normal section for monoclinic flows (Passchier, 1997). Similar to Truesdell's kinematic vorticity number (Truesdell, 1953), the dilatancy number, A_k, can be reformulated as a measure of three-dimensional volume change rate by normalizing δ against the intensity of stretching Γ as in Jiang (1994b):

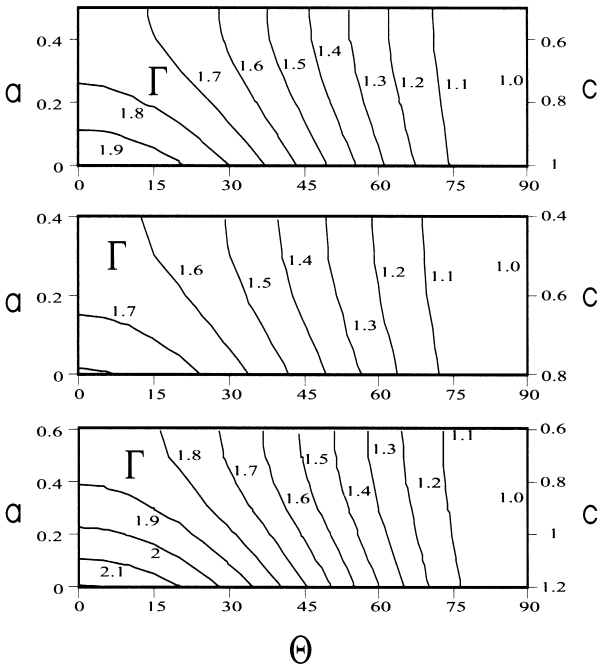

Fig. 2. The effective shear strain rate (intensity of stretching), Γ, normalized with respect to the velocity gradient E as a function of Θ, a and c for isochoric (top), volume decrease (middle) and volume increase (bottom) situations. See text for details.

$$A_k = \frac{\delta}{[2(\dot{\epsilon}_a^2 + \dot{\epsilon}_b^2 + \dot{\epsilon}_c^2 + \frac{1}{2}\dot{\gamma}^2)]^{\frac{1}{2}}} = \frac{1 - a - c}{[2(a^2 + c^2 + 1 + \frac{1}{2}\tan^2\Theta)]^{\frac{1}{2}}}. \quad (10)$$

$A_k > 0$, $A_k < 0$ and $A_k = 0$ represent flow that is divergent (volume increasing), convergent (volume decreasing) and isochoric (constant volume), respectively (Jiang, 1994b). Figure 3 shows A_k as a function of a, c and Θ for $a + c = 0.8$ and $a + c = 1.2$. For the same material and same accommodating deformation, $\Theta \to 0$ will result in faster volume change than $\Theta \to 90$. For bulk simple shear deformation ($\Theta = 90$), the deformation is isochoric.

Similarly, Truesdell's kinematic vorticity number of flow W_k is: (Fig. 4)

$$W_k = \frac{\dot{\gamma}}{[2(\dot{\epsilon}_a^2 + \dot{\epsilon}_b^2 + \dot{\epsilon}_c^2 + \frac{1}{2}\dot{\gamma}^2)]^{\frac{1}{2}}} = \frac{\tan\Theta}{[2(a^2 + c^2 + 1 + \frac{1}{2}\tan^2\Theta)]^{\frac{1}{2}}}. \quad (11)$$

Truesdell defined the kinematic vorticity number in order to measure the degree of rotation of a flow. The limitation of this (frame dependence) is discussed in Astarita (1979) and Means *et al.* (1980).

The sectional kinematic vorticity number, W_k^s, (Passchier, 1988, 1990, 1991; Robin and Cruden, 1994) on the vorticity-normal section (VNS) is obtained with a Mohr circle construction (Fig. 5):

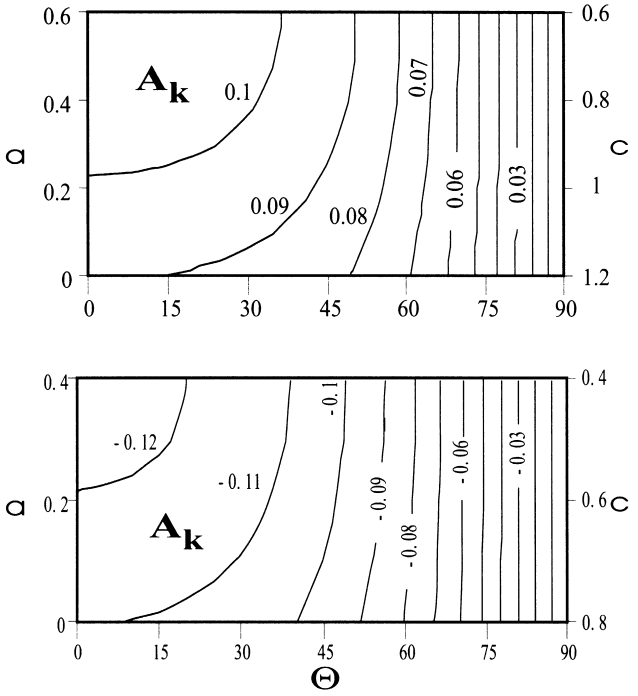

Fig. 3. The kinematic dilatancy number A_k as a function of Θ, a and c for volume increase (top) and volume decrease (bottom) situations.

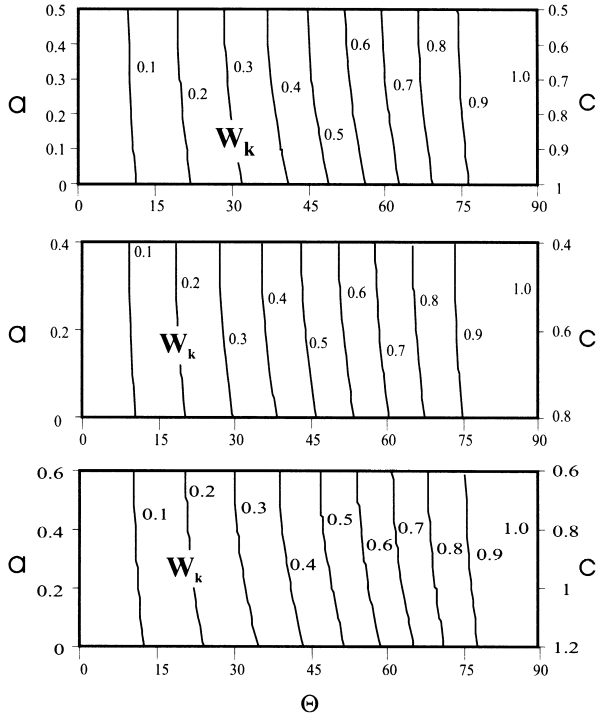

Fig. 4. Truesdell's kinematic vorticity number as a function of Θ, a and c for isochoric (top), volume decrease (middle) and volume increase (bottom) situations.

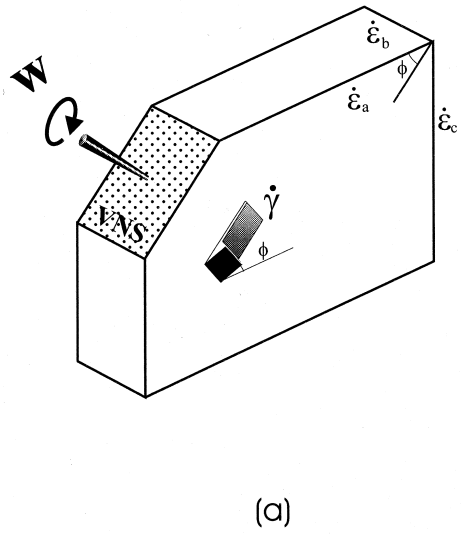

(a)

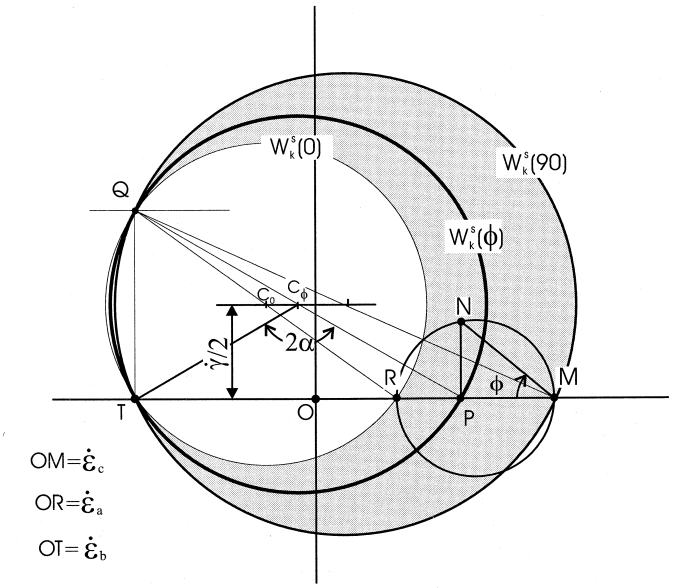

(b)

Fig. 5. Mohr circle construction for the sectional kinematic vorticity number W_k^s on the VNS. (a) Geometrical relationship between the vorticity vector, **W**, VNS (shaded) and shear direction. (b) Mohr circle for the flow in a general high-strain zone. The two-dimensional flow on the x_1x_3 plane (Fig. 1) is represented by the circle MNR centered on the horizontal axis, $OR=\dot{\varepsilon}_a$ and $OM=\dot{\varepsilon}_c$. The material line instantaneously parallel to the shear direction is plotted at N on circle MNR. Therefore stretching along it is represented by OP on the horizontal axis, where NP is perpendicular to the horizontal axis. The stretching of the material line instantaneously normal to the zone boundary is $OT=\dot{\varepsilon}_b$ (recall that $\dot{\varepsilon}_b$ has opposite sign to $\dot{\varepsilon}_a$ and $\dot{\varepsilon}_c$). This, together with the shearing $\dot{\gamma}$, gives a point Q ($\dot{\varepsilon}$, $\dot{\gamma}$). PQ is a diameter of the Mohr circle for the two-dimensional flow on the VNS. From this circle W_k^s can be readily obtained by $W_k^s=\cos\alpha$. It is seen that as ϕ varies from 0° to 90°, the Mohr circle for the flow on the VNS varies within the shaded area. C_0, C_ϕ and C_{90} are centers of the Mohr circles for $\phi = 0°$, $0° < \phi < 90°$ and $\phi = 90°$ respectively. W_k^s reaches a maximum when $\phi = 0°$ and a minimum when $\phi = 90°$.

$$W_k^s = \frac{\dot{\gamma}}{[\dot{\gamma}^2 + (\dot{\epsilon}_a \cos^2\phi + \dot{\epsilon}_c \sin^2\phi - \dot{\epsilon}_b)^2]^{\frac{1}{2}}} = \frac{\tan\Theta}{[\tan^2\Theta + (1 + a\cos^2\phi + c\sin^2\phi)^2]^{\frac{1}{2}}}. \quad (12)$$

Figure 6 shows W_k^s as a function of Θ, a and ϕ for isochoric flow ($a + c = 1$), (Fig. 6a), and examples of convergent ($a + c = 0.8$) (Fig. 6b) and divergent ($a + c = 1.2$) (Fig. 6c) flow situations.

The physical significance of W_k^s is easily understood for steady monoclinic flows where the VNS is attached to a single material plane throughout deformation. The VNS is where the maximum asymmetry of the fabric is to be observed, whether the fabric records a finite deformation or instantaneous deformation. For triclinic flows, a material plane coincident with the VNS at an instant will immediately rotate away from it as deformation advances. Thus the section of a rock sample on which maximum asymmetry is observed is generally not the VNS if the flow is triclinic. A spiral inclusion trail in a *spherical* garnet is an exception. The axis of such a spiral is always perpendicular to the VNS, irrespective of the symmetry of the flow so long as the flow is steady. For a fabric that reflects an accumulated deformation, as most fabrics do, the correlation of W_k^s with the symmetry of the fabric is not well understood. In fact as we will show in the following (see also Lin *et al.*, 1998), a triclinic flow may produce an apparent monoclinic structural geometry if there is a large component of simple shear in the flow.

It has been shown that five independent parameters are needed to completely characterize the flow of our model. However, if we are only interested in the kinematic characteristics of the flow ('flow geometry' of Passchier and Trouw, 1996) rather than the actual rate of deformation, then only four independent parameters are needed, such as the set: Θ, ϕ, a and c. Two flows identical in the above four parameters are identical in terms of kinematics, despite possible difference in their rate of deformation (to include the rate, an additional parameter, any one of E, $\dot{\epsilon}_b$ or $\dot{\gamma}$, is needed). The temporal evolution of these four characteristic parameters defines the kinematic history of a high-strain zone.

FINITE DEFORMATION GEOMETRY

The position gradient tensor

We now present the position gradient tensor $\mathbf{F}(t)$ for the finite deformation within a general high-strain zone in terms of the characterizing parameters (E, Θ, ϕ, a and c). The differential equations embedded in (5) are:

$$\frac{Dx_1}{Dt} = \dot{\epsilon}_a x_1 + \dot{\gamma}\cos\phi x_2$$
$$\frac{Dx_2}{Dt} = \dot{\epsilon}_b x_2 \quad (13)$$
$$\frac{Dx_3}{Dt} = \dot{\gamma}\sin\phi x_2 + \dot{\epsilon}_c x_3.$$

The solutions to (13) are considered for two situations.

Homogeneous and steady deformations or deformations divisible into homogeneous domains and steady periods. For a homogeneous and steady deformation, the strain rates on the right sides of equations (13) are constants. In such a case, equations (13) can be analytically integrated (e.g. Jeffrey, 1995) to give relationships between the initial coordinates (X_1, X_2, X_3) and the final coordinates (x_1, x_2, x_3) in the forms of $x_i = x_i$ (X_1, X_2, X_3), (i = 1, 2, 3). The position gradient tensor $\mathbf{F}(t)$, whose components are $F_{ij} = \partial x_i/\partial X_j$, can be obtained accordingly as follows:

$$\mathbf{F}(t) = \begin{pmatrix} \exp(-a\cdot E\cdot t\cdot\cos\Theta) & \frac{\tan\Theta\cos\phi}{1+a}[\exp(E\cdot t\cdot\cos\Theta) - \exp(-a\cdot E\cdot t\cdot\cos\Theta)] & 0 \\ 0 & \exp(E\cdot t\cdot\cos\Theta) & 0 \\ 0 & \frac{\tan\Theta\sin\phi}{1+c}[\exp(E\cdot t\cdot\cos\Theta) - \exp(-c\cdot E\cdot t\cdot\cos\Theta)] & \exp(-c\cdot E\cdot t\cdot\cos\Theta) \end{pmatrix} \quad (14a)$$

$$(\Theta \neq 90^\circ),$$

or:

$$\mathbf{F}(t) = \begin{pmatrix} 1 & E\cdot t\cdot\cos\phi & 0 \\ 0 & 1 & 0 \\ 0 & E\cdot t\cdot\sin\phi & 1 \end{pmatrix} \quad (\Theta = 90^\circ). \quad (14b)$$

As a function of E, Θ, ϕ, a, c and t, $\mathbf{F}$ can be written as $\mathbf{F}(E, \Theta, \phi, a, c, t)$. Suppose a natural heterogeneous and non-steady deformation is divisible into a number of homogeneous domains. In each domain, the deformation is divided into n time intervals, within each the deformation being steady. The first incremental deformation accumulated during the time span $0 \sim t_1$ is: $\mathbf{F}_1^0 = \mathbf{F}(E_1, \Theta_1, \phi_1, a_1, c_1, t_1)$, and the incremental deformation for the time period $t_{i-1} \sim t_i$ can be generally written as:

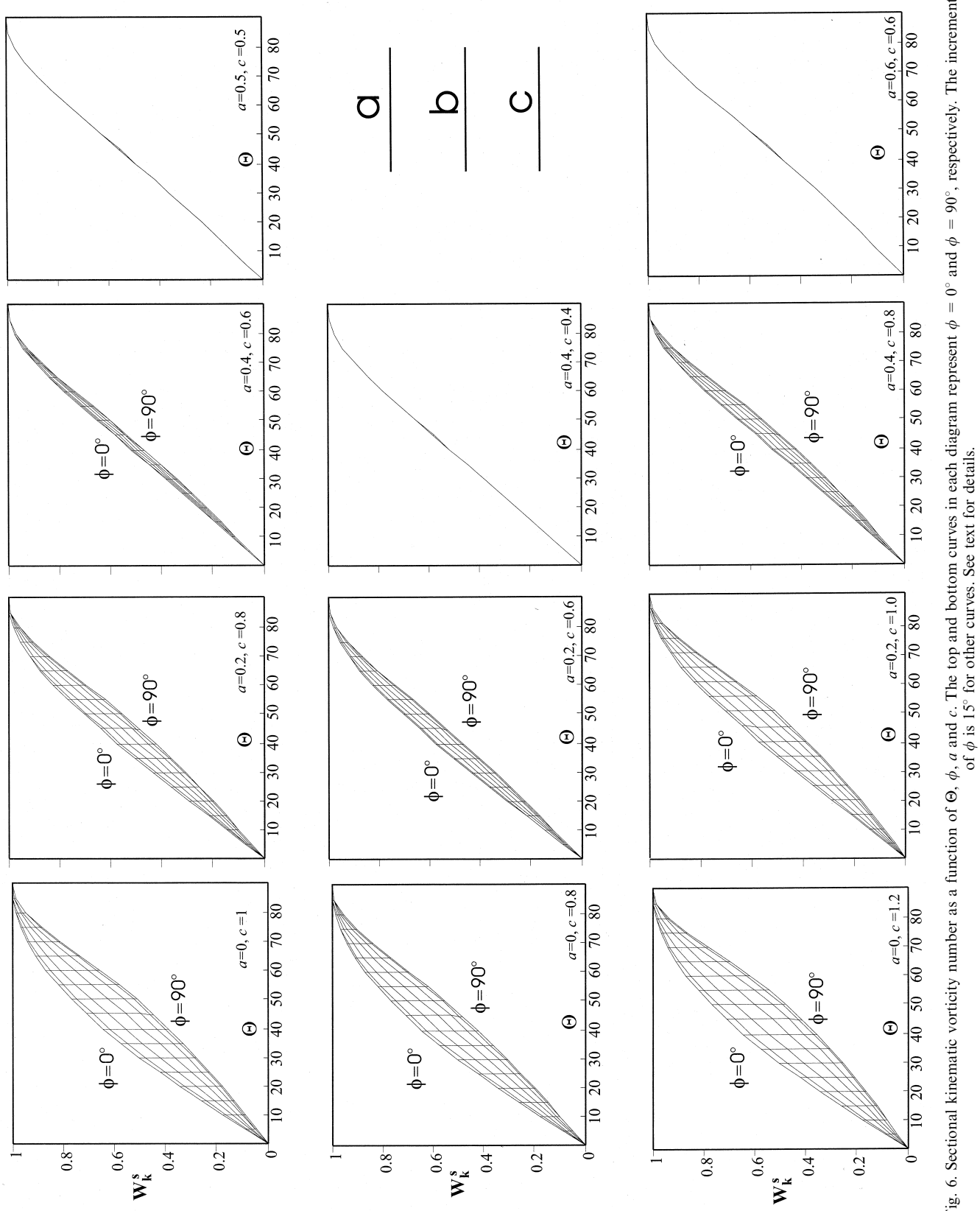

Fig. 6. Sectional kinematic vorticity number as a function of Θ, ϕ, a and c. The top and bottom curves in each diagram represent $\phi = 0^\circ$ and $\phi = 90^\circ$, respectively. The increment of ϕ is 15° for other curves. See text for details.

$$\mathbf{F}_i^{i-1} = \mathbf{F}(E_i, \Theta_i, \phi_i, a_i, c_i, t_i - t_{i-1}), \tag{15}$$

where the superscript and subscript represent the end and the starting configurations, respectively, during each time interval. The total accumulated finite deformation is then determined by tensor multiplication (e.g. Elliott, 1972), i.e.:

$$\mathbf{F} = \mathbf{F}_n^{n-1} \cdot \mathbf{F}_{n-1}^{n-2} \cdot \mathbf{F}_{n-2}^{n-3} \cdot \ldots \cdot \mathbf{F}_1^0. \tag{16}$$

Flow as a function of time can be approximated by analytical expressions. When flow varies with time, analytical integration of equation (13) is generally impossible. However, **F** can be obtained numerically. Numerical integration can be carried out in various ways. If flow variation, which can be represented by the variation of the five characterizing parameters, can be approximated by analytical expressions, the Runge–Kutta–Gill method is the obvious choice. If flow variation can only be expressed numerically and it is not possible to choose constant time intervals for integration, other methods must be used.

If $\mathbf{F}(t)$ at time $n\Delta t$ is written as $\mathbf{F}_n$, **F** can be obtained by the following circulation (McKenzie, 1979; Dutton, 1997):

$$\mathbf{F}_{n+1} = \mathbf{A}^{-1}\mathbf{B}\mathbf{F}_n \tag{17}$$

where **A** and **B** are tensors whose components are:

$$A_{ij} = \delta_{ij} - 1/2\Delta t L_{ij},\ B_{ij} = \delta_{ij} + 1/2\Delta t L_{ij}$$
(δ is the Kronecker delta). (18)

When sufficiently detailed work has been carried out and the deformation path is well constrained, some form of analytic curves (e.g. exponential or polynomial curves) could be used to fit the observed data of a natural deformation and then used for numerical integration. Alternatively, natural variation can be modelled theoretically. For example, White (1994) used an exponential function to model the increase and decrease of natural strain rates. Once a heterogeneous and non-steady flow history is approximated by analytic expressions, equations (17) and (18) can be used to determine the finite deformation.

Before more complex deformation paths are examined using equations (14)–(18), the behavior of the simplest deformational histories needs to be understood. Thus we present results for homogeneous and steady deformations.

The accumulation of finite strain

The finite strain can be calculated by taking the eigenvalues of the 'left Cauchy–Green tensor', $\mathbf{F}\mathbf{F}^{\mathrm{T}}$ (Truesdell and Toupin, 1960). The eigenvalues are the three principal quadratic elongations λ_1, λ_2 and λ_3 ($\lambda_1 \geq \lambda_2 \geq \lambda_3$), the squares of the three principal stretches, whereas the corresponding eigenvectors are the orientations of the principal strain axes in the deformed state.

Because we are dealing with three-dimensional finite strain, one of Lode's numbers, ε_s, is used to represent the strain state. It is as defined by Nadai (1963):

$$\varepsilon_s = \sqrt{\frac{1}{3}[(\varepsilon_1 - \varepsilon_2)^2 + (\varepsilon_2 - \varepsilon_3)^2 + (\varepsilon_3 - \varepsilon_1)^2]}, \tag{19}$$

where $\varepsilon_i = 1/2 \ln \lambda_i$ (i = 1, 2, 3) are the principal natural strains. Given a velocity gradient across a high-strain zone, the finite strain within the zone, ε_s, accumulates at different rates depending on Θ, ϕ and a (because ε_s is independent of volume change, it depends on either a or c not both) (Fig. 7). The finite strain accumulates most efficiently when $\Theta = 0^\circ$ (pure shear), and least efficiently when $\Theta = 90^\circ$ (simple shear). For the same Θ, an increase in a will slow down the rate of accumulation (yellow areas in Fig. 7). For flows of monoclinic or higher symmetry ($\Theta = 0^\circ$, 90°, and $a = c$), the rate of accumulation becomes independent of ϕ (Fig. 7). For triclinic flows, the rate of accumulation increases as ϕ decreases (Fig. 7). A decrease in ϕ corresponds to an increase in W_k^s (Fig. 6).

Evolution of the principal strain axes

The orientations of the principal strain axes can be readily calculated by taking the eigenvectors of the left Cauchy–Green tensor (Truesdell and Toupin, 1960). The pattern and time evolution of λ_1 can be used to represent the variation across a high-strain zone of finite-strain-related lineations, such as those stretching lineations defined by shape fabrics (discussed later). Similarly the λ_1–λ_2 plane can be used to approximate the finite-strain-related foliations and λ_3 the poles to the foliations.

Figures 8–11 are lower hemisphere projections showing the evolution with time of the orientation of the principal finite strain axes λ_1 and λ_3 for thinning zones (Figs 8, 9 & 11) and thickening zones (Fig. 10) for various Θ, ϕ, a and c values. Each stereographic diagram in Figs 8–11 is a composite one with respect to Θ. For any set of parameters, the principal strain axes start with the instantaneous stretching axes (ISA) (t = 0, the first symbol) and gradually change orientations as the finite strain increases (indicated by the thick arrow). Characteristic features of Figs 8–11 can be summarized as follows.

1. The finite strain geometry for thinning zones (Figs 8–10) and for thickening zones (Fig. 11) exhibits such a symmetry that statements made for λ_1 and λ_3 in thinning zones are generally true, respectively, for λ_3 and λ_1 in thickening zones.

2. For monoclinic deformation paths ($\Theta = 90^\circ$, $\phi = 0^\circ$, 90° or $a = c$), λ_1 and λ_3 plot on the VNS and as strain increases, λ_1 approaches the shear direction

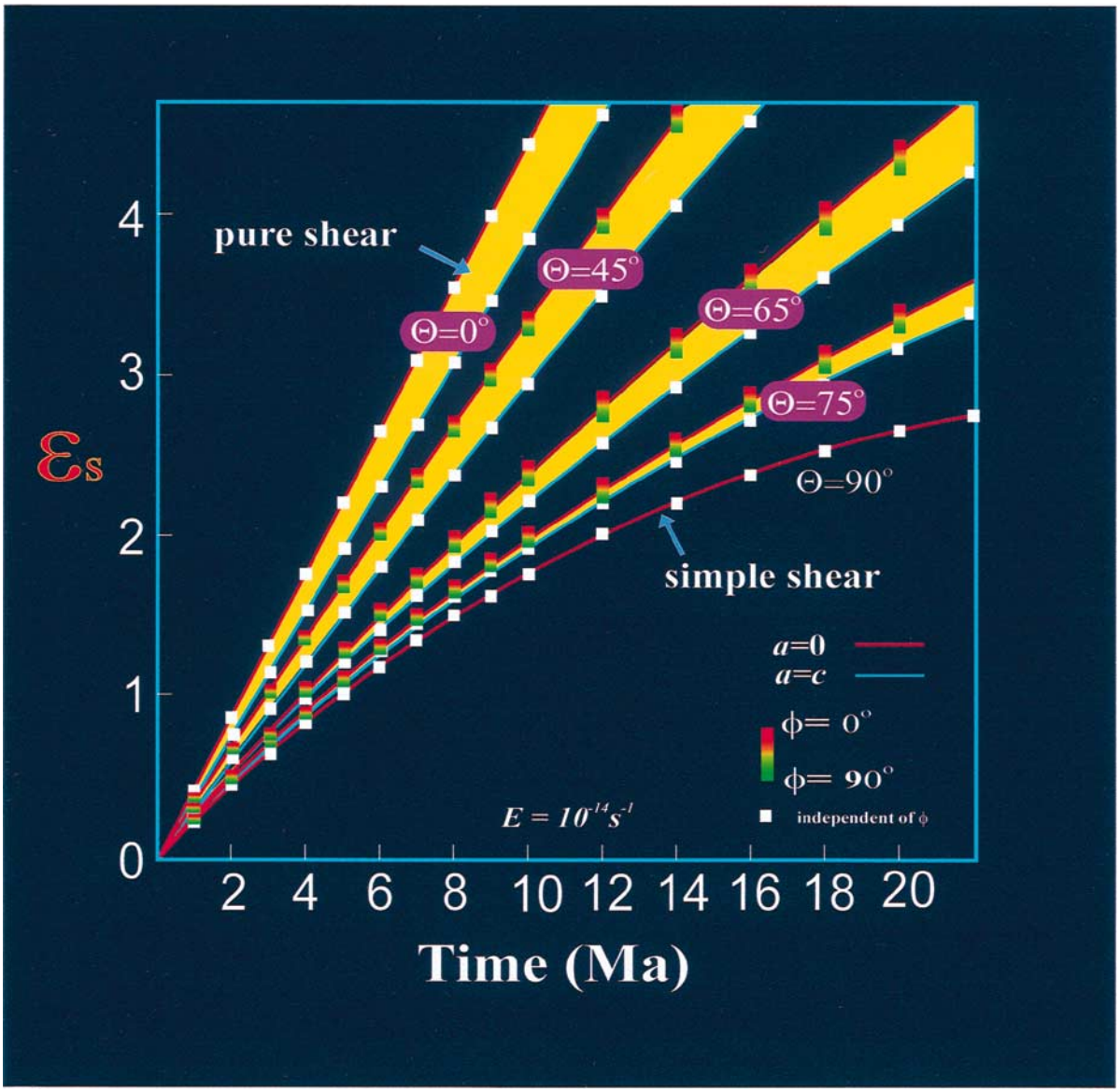

Fig. 7. Finite strain accumulation with time: Lode's number, ε_s, as a function of Θ, a and ϕ for a velocity gradient $E = 10^{-14}$ s^{-1} across the zone. Five situations are presented: pure shear ($\Theta = 0°$), sub-simple shear ($\Theta = 45°$, 65°, 75°) and simple shear ($\Theta = 90°$). For each situation, the upper limit red line represents $a = 0$ and the lower limit blue line represents $a = c$. The yellow area represents $0 < a < c$. ε_s is independent of volume change. The effect of varying ϕ is shown by the vertical bar for each plot. Where $a = c$ or $\Theta = 90°$, the deformation is monoclinic and is independent of ϕ as is intuitively obvious.

progressively ($\phi = 0°$, 90° situations in Fig. 8B & 11A, and the situation of $a = c$ Fig. 9B). For a thinning zone, the end orientation of λ_1 is the shear direction (Fig. 8B, $\phi = 0°$ and 90°, Fig. 9B). For a thickening zone, the end orientation of λ_1 is the extensional flow apophysis lying on the VNS but makes an angle ($=\cos^{-1} W_k^s$, Bobyarchick, 1986) with respect to the shear direction (Fig. 11, $\phi = 0°$ and 90°).

3. For a thinning zone with triclinic symmetry, λ_1 plots away from the VNS. As strain increases, λ_1 rotates via a curved path. The end orientations for λ_1 are the orientation of $\dot{\epsilon}_c$, not the shear direction. The closer the deformation is to being monoclinic [i.e. $\Theta \rightarrow 90°$ (e.g. $\Theta = 80°$, 85°), $\phi \rightarrow 0°$, 90° $a \rightarrow c$], the longer (higher strain) path λ_1 takes to approach the orientation of $\dot{\epsilon}_c$. As $\Theta \rightarrow 90°$, λ_1 stays close to the VNS and rotates towards the shear direction at low and intermediate strains. At higher strains it swings away from the VNS trace and follows the HSZB trace toward $\dot{\epsilon}_c$ (Figs 8–11, all cases with $\Theta = 85°$). When $\Theta \leq 45°$, λ_1 plots very close to the orientation of $\dot{\epsilon}_c$ throughout the history. If ϕ approaches 0° or 90° in these situations, the strain geometry becomes not much different to that resulting from an orthorhombic deformation path (e.g. Figs 8C & 9A, $\phi = 10°$, $\Theta = 45°$). As a increases, all λ_1 loci converge on the VNS until when $a = c$, all λ_1 loci plot on the VNS (Fig. 9A). This is because an increase in a makes the symmetry closer to being monoclinic. Although λ_3 never plots exactly on the VNS for triclinic paths,

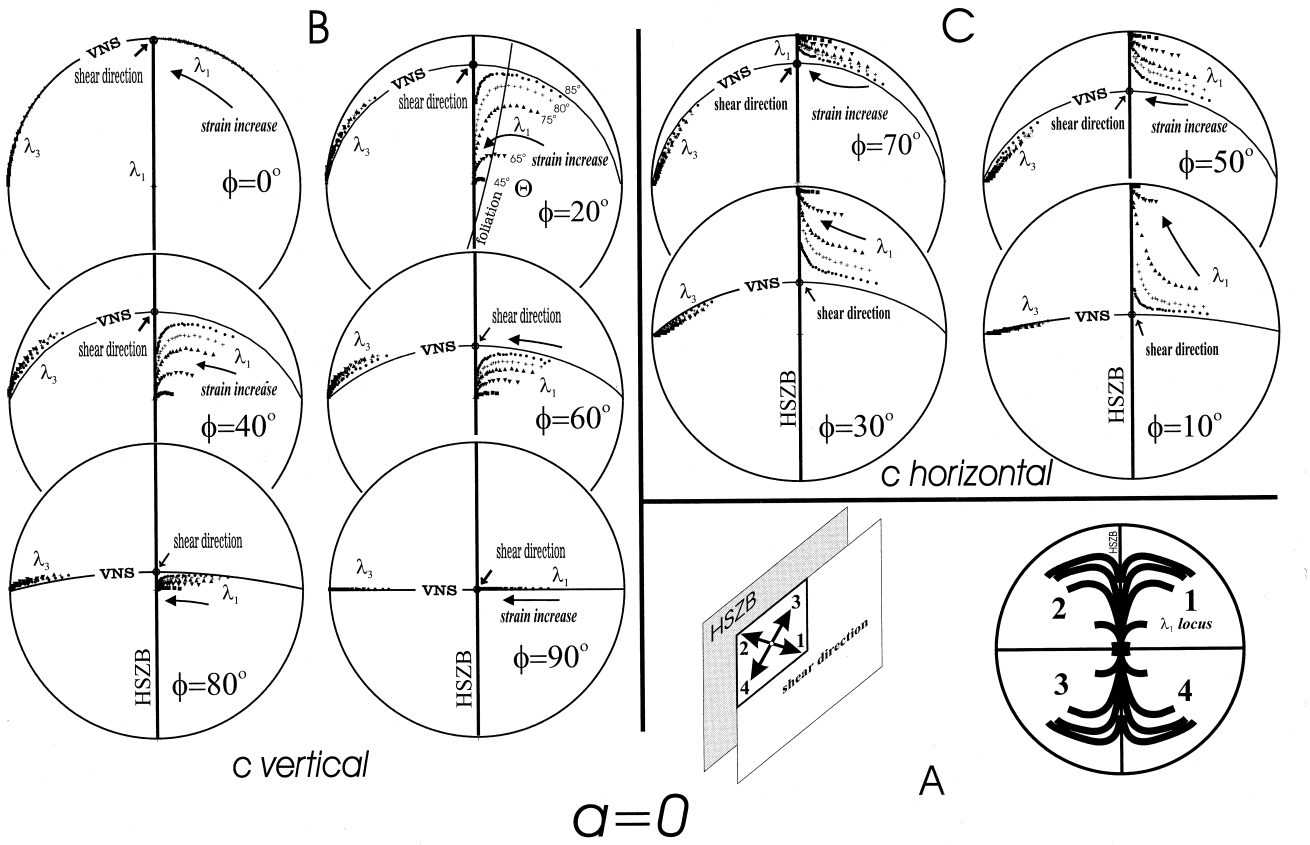

Fig. 8. Equal-area lower-hemisphere projection of variation and evolution with progressive deformation of the maximum (λ_1) and minimum (λ_3) principal finite strain axes for thinning zones. (A) Correspondence between the movement of a high-strain zone in real space and the locus of λ_1 in the stereographic space for both thinning and thickening zones. (B) Isochoric deformation with $a = 0$, $c = 1$ and c vertical. (C) Isochoric deformation with $a = 0$, $c = 1$ and c horizontal. When $\Theta \neq 90°$ and $a \neq c$, the strain geometry is triclinic, but appears monoclinic as $\Theta \rightarrow 90°$. Irrespective of Θ, ϕ, a and c, λ_3 always plots close to the VNS. Solid square, solid triangle apex up, solid triangle apex down, cross and solid circle stand for $\Theta = 45°$, 65°, 75°, 80° and 85°, respectively. VNS = vorticity-normal section. HSZB = high-strain zone boundary.

unlike λ_1, it *always* plots close to the VNS for all cases.

4. For a thickening zone in a triclinic situation, the reverse is true: λ_1 plots very close to the VNS trace whereas λ_3 plots away from it. This property can be used to find the vorticity vector for a thickening zone. Unlike a thinning zone where the end orientation of λ_1 is the direction of $\dot{\epsilon}_c$, the extensional apophysis for a thickening zone is inclined to the boundary. The contrasting features between a thinning zone and a thickening can be used to tell them apart.

5. For situations with $\dot{\epsilon}_a \cdot \dot{\epsilon}_c \geq 0$, thinning zones produce oblate strains ($K < 1$), thickening zones produce prolate strains ($K > 1$) and constant-thickness zones produces plane strains ($K = 1$) (Fig. 12).

6. Volume change has little affect on the geometry (Fig. 8B). In fact, it would be impossible to infer volume change solely on the basis of strain geometry.

DISCUSSION

Potential applications

There are advantages in taking a general approach towards high-strain zones. In the unified model, the instantaneous flow is described by a single velocity gradient tensor (equation 5) and the finite deformation for a homogeneous domain and steady period is described by a single position gradient tensor (equation 14). Since the model covers deformation paths ranging from coaxial to monoclinic non-coaxial to triclinic non-coaxial, one can potentially use the two tensors to investigate a very wide range of deformations. The stretch and rotation history of a material line can readily be investigated using these tensors. For example, the stretch history of a material line $\lambda^{1/2}(t)$ whose initial orientation is represented by a unit vector

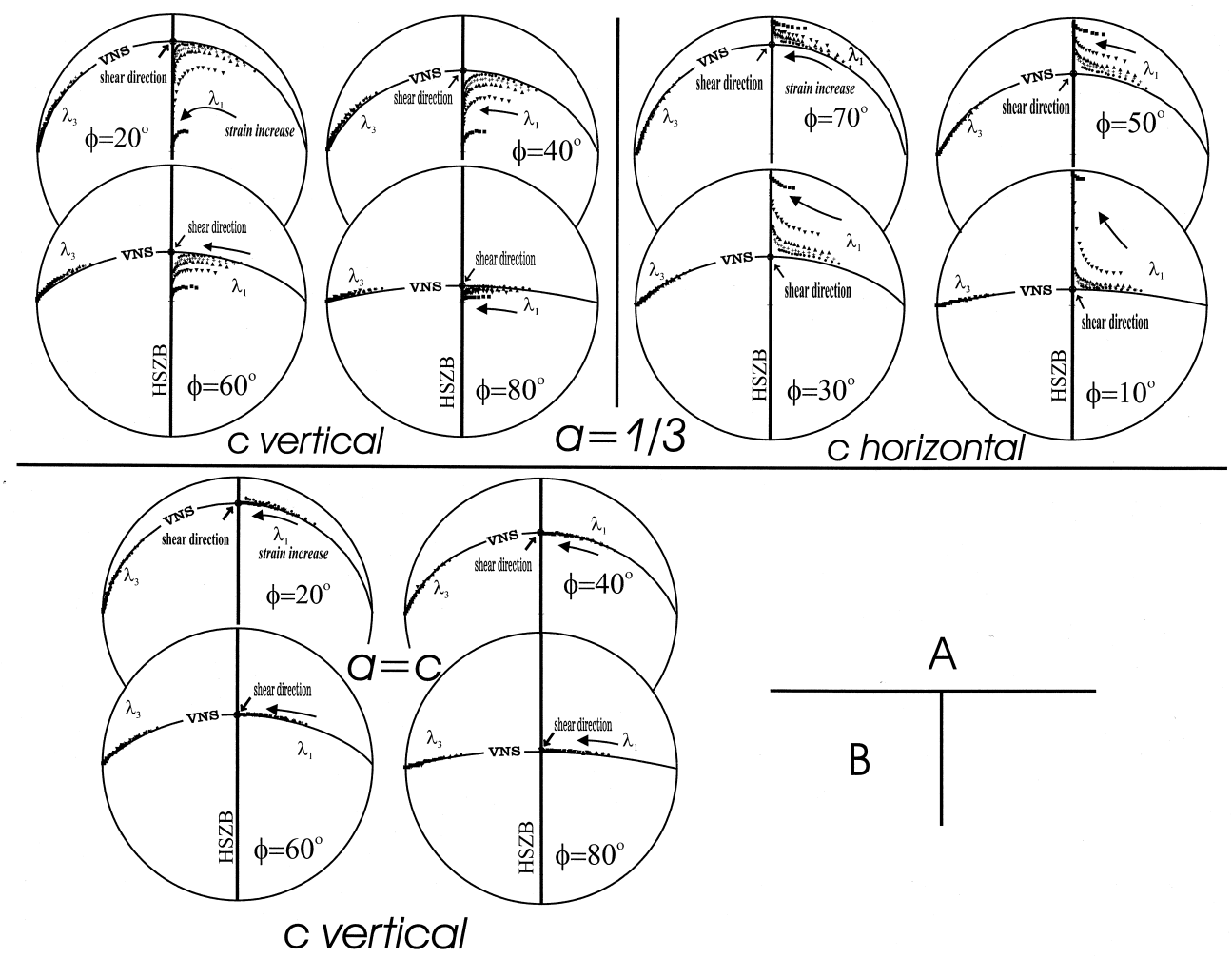

Fig. 9. Equal-area lower-hemisphere projection of variation and evolution with progressive deformation of the maximum (λ_1) and minimum (λ_3) principal finite strain axes for thinning zones. (A) Isochoric deformation with $a = 1/3$ and $c = 2/3$. (B) Situations where $a = c$ irrespective of volume change. When $\Theta \neq 90^\circ$ and $a \neq c$, the strain geometry is triclinic, but appears monoclinic as $\Theta \rightarrow 90^\circ$. Irrespective of Θ, ϕ, a and c, λ_3 always plots close to the VNS. Symbols are the same as in Fig. 8.

$\mathbf{N} = (N_1, N_2, N_3)$ in the reference frame of Fig. 1 is simply (Truesdell and Toupin, 1960):

$$\lambda_{\mathbf{N}}^{\frac{1}{2}}(t) = \sqrt{N_j N_k F_{ij}(t) F_{ik}(t)}, \tag{20}$$

where the repeated subscript means summation over the values 1, 2 and 3 of that subscript. Using equation (20), the stretch history for any line can be constructed in a form such as in fig. 2.11 of Passchier and Trouw (1996, p. 18) for any given deformation path. Similarly, the rotation history of material lines and planes can also be investigated using the position gradient tensor. We have constructed the material line rotation loci maps for different deformation paths and have used them to investigate the evolution of the geometry of folds in high-strain zones.

The model can also be used to compare structural and fabric geometries observed from natural high-strain zones with the model results presented in this paper and constraints placed on possible deformation paths, as in Lin *et al.* (1998). For example variably oriented lineations and consistently oriented foliations in a high-strain zone (Goodwin and Williams, 1996; Lin *et al.*, 1998) suggests that the zone is thinning, whereas consistently oriented lineations and variably oriented foliations suggests a zone is thickening. The geometrical property that λ_3 for a thinning zone and λ_1 for a thickening zone always plot close to the VNS whether the deformation path is triclinic or monoclinic can be used to constrain the vorticity vector for a high-strain zone. *The intersection between the zone boundary and a finite-strain-related foliation in a thinning zone, and the intersection between the zone boundary and the plane normal to lineations in a thickening zone, approximately define the vorticity vector.*

Some conclusions based on monoclinic models need modification before being applied to general situations. For example the fact that λ_1 plots away from the VNS for triclinic thinning zones clearly shows that the statement that stretching lineations will align with and

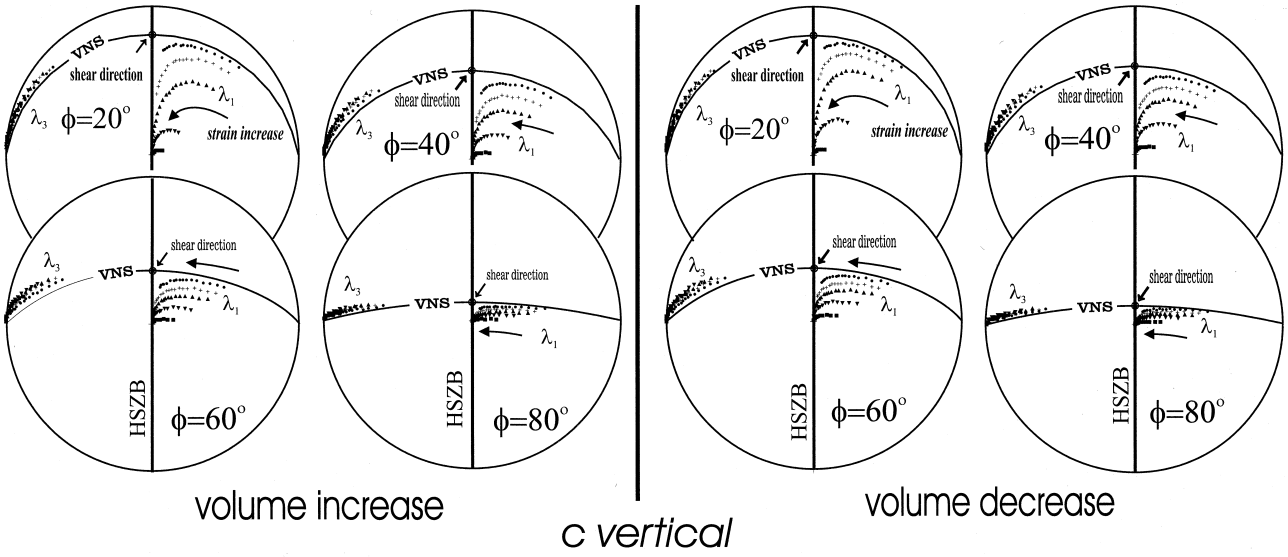

Fig. 10. Equal-area lower-hemisphere projection of variation and evolution with progressive deformation of the maximum (λ_1) and minimum (λ_3) principal finite strain axes for thinning zones where volume changes are involved ($a = 0$, $c = 1.2$ for volume increase; $a = 0$, $c = 0.8$ for volume decrease). c is set vertical. When $\Theta \neq 90°$ and $a \neq c$, the strain geometry is triclinic, but appears monoclinic as $\Theta \rightarrow 90°$. Irrespective of Θ, ϕ, a and c, λ_3 always plots close to the VNS. Symbols are the same as in Fig. 8.

therefore indicate the shear direction cannot be extrapolated to general high-strain zones, even if the lineation represents the principal strain axes.

Nature of lineations and foliations in high-strain zones

Figures 8–11 present the orientation history of the principal finite strain axes. How they relate to lineations and foliations is not a simple subject. It is important to understand the nature of lineations and foliations and the mechanisms involved in their formation before interpreting them kinematically. In non-coaxial deformation there are such complications as the inability of material lines and surfaces to track finite strain axes (Williams *et al.*, 1977; Hobbs *et al.*, 1982) and the problem of steady state fabrics (Means, 1981). This problem which has been discussed extensively with respect to foliations (Williams, 1976; Hobbs *et al.* 1982; Treagus, 1983) is just as acute in the interpretation of lineations. Lineations are commonly interpreted as representing the maximum principal strain axis despite a lack of cogent evidence (see however Goodwin and Williams, 1996). A lineation defined by deformed objects such as ooids in an oolitic limestone or by pebbles in a conglomerate may closely track the principal strain direction so long as the rheological contrast is negligible. However, if the deforming objects are grains in, for example, a monomineralic aggregate then recrystallization may continually restore the shape of the most deformed grains to a more equant form. A competition will ensue between the lineation-producing deformation and the lineation-annihilating recrystallization resulting in a steady state lineation (Means, 1981) that will lie at some fixed point on an appropriate path in Figs 8–11, somewhere between the ISA and the principal finite strain axes. If the deformation path is monoclinic the normal to the steady-state foliation will lie on or normal to the VNS as do the maximum ISA and the maximum principal finite strain axis. The steady-state lineation will either lie on the VNS or parallel to the vorticity vector depending on the nature of the flow. In triclinic flow however, there is no special relationship.

Lineations defined by rotated grains with elongate habit, such as plagioclase crystals in a melt or sillimanite crystals in a metamorphic rock are different again. If their initial orientation distribution is uniform-random their preferred orientation may track a principal axis, but interference between grains and initial preferred orientation patterns will complicate the picture. So for example, if there is an initial preferred planar orientation of the grains they will be unable to track strain axes but will converge on the extensional flow apophysis.

Yet another type of lineation found in shear zones is ridge-in-groove slickenside striae (Means, 1987). This can be a penetrative fabric element (Lin and Williams, 1992) and it forms parallel to the local shear direction. Having formed, if the flow is triclinic the lineation may rotate towards the extensional flow apophysis or, if the lineation is on a foliation parallel to the zone boundary (such as the *C*-plane), it will rotate toward the maximum stretching direction ($\dot{\varepsilon}_c$ direction) of the boundaries.

Finally, even though linear elements may track local kinematic axes they may not reflect the bulk deformation path. For example Williams and Vernon (in press) have shown how a grain shape fabric may be inclined to the principal strain axes due to grain scale partitioning of the strain. In their model, shear zone

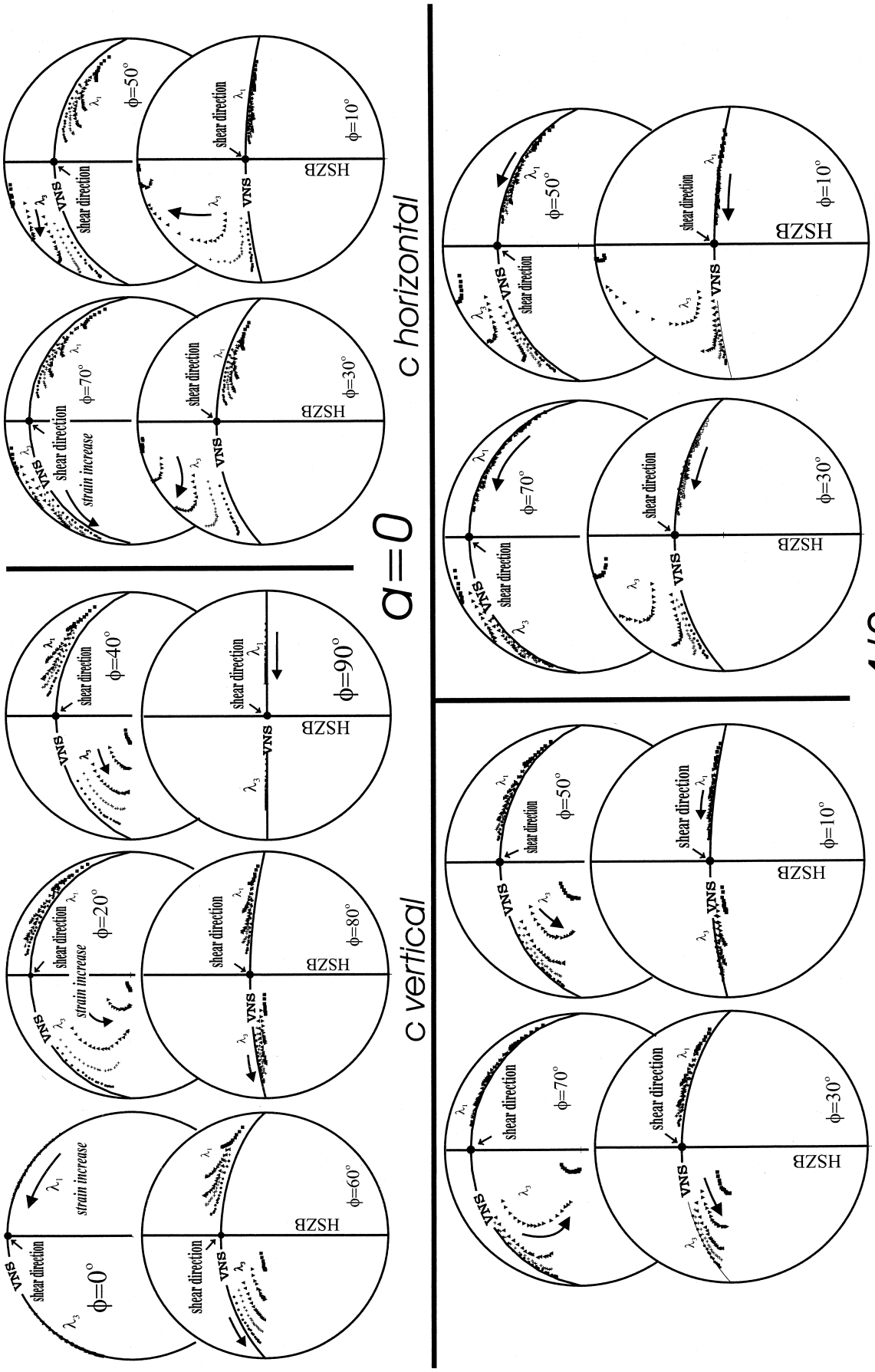

Fig. 11. Equal-area lower-hemisphere projection of variation and evolution with time of the maximum (λ_1) and minimum (λ_3) principal finite strain axes for thickening zones with varying Θ, ϕ, a and c. Symbols are the same as in Fig. 8. (a) Isochoric deformation with $a = 0$ and $c = 1$. (b) Isochoric deformation with $a = 1/3$ and $c = 2/3$. For all situations whereas λ_3 varies in orientation, λ_1 always plots close to the VNS. Compare with Fig. 8 to see the contrasting features between a thinning zone and a thickening zone and see text for further discussion.

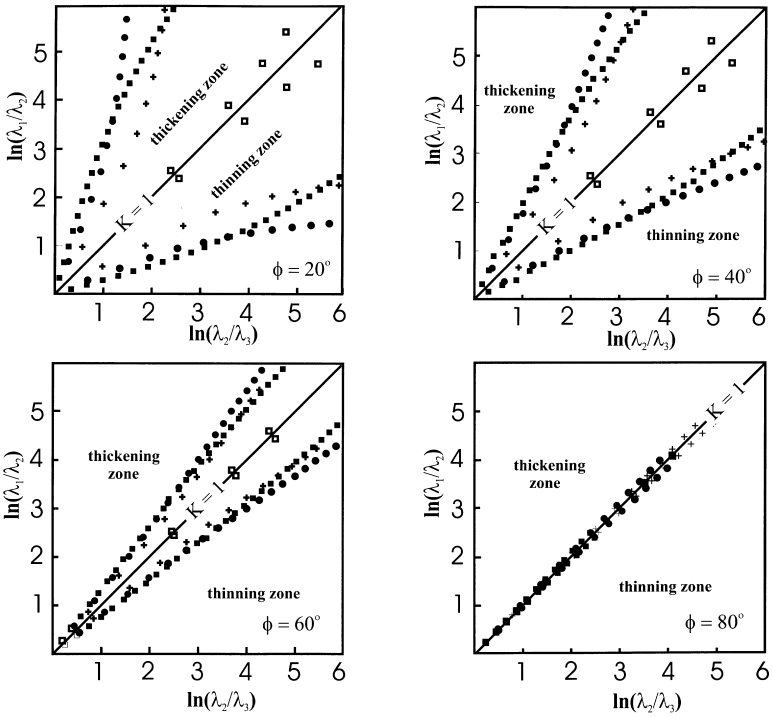

Fig. 12. Plots of the shapes of the finite strain ellipsoids for thinning and thickening zones with $a=0$ and $c=1$ for different ϕ values. Thinning zones produce oblate strains ($K<1$), thickening zones produce prolate strains ($K>1$) and constant-thickness zones produce plane strain ($K=1$). Plots for thinning zone and thickening zone are symmetric about the line defined by $K=1$. Solid square, solid circle, cross and open square represent $\Theta = \tan^{-1}(\dot{\gamma}/\dot{\epsilon}) = \tan^{-1}2$, $\tan^{-1}4$, $\tan^{-1}6$ and $\tan^{-1}10$, respectively.

parallel shear is achieved by sliding on grain boundaries and does not influence grain shape. A pure shear component of strain, which cannot be accommodated by grain boundary sliding, results in stretching of the grains parallel to the principal axis for the pure shear component. This grain scale stretching direction is inclined to the bulk strain principal stretching direction by up to 90°.

Significance of triclinic deformation paths in nature

At this stage, the question has to be asked: Do we really need to be concerned with triclinic deformation paths? In the Introduction we mentioned that boundary conditions favorable to triclinic deformation are common in nature. On the largest scale, observations of present plate motions reveal that boundaries are commonly transpressive (Harland, 1971) and that the oblique plate velocity vector is heterogeneously accommodated as a result of slip partitioning (e.g. Liu *et al.*, 1995); i.e. the net oblique velocity is partitioned into a more dip-slip component at the subduction zone plus an intraplate component in the overriding and underriding plates (e.g. Fitch, 1972; DeMets, 1992; McCaffrey, 1992; Shen-Tu *et al.*, 1995). The intraplate deformation shows further partitioning (e.g. Gao and Wallace, 1995). However, a complete partitioning where the net slip is partitioned into two end members: pure dip-slip and pure strike slip components, as argued in e.g. Tikoff and Teyssier (1994), may be rare. Generally the shear direction is oblique, $0° < \phi < 90°$ (e.g. Liu *et al.*, 1995), which, combined with stretching boundaries, will lead to triclinic deformation paths. This is likely to be a common situation. On the scale of a single deformation zone, oblique slip is very common in natural faults and high-strain zones. Where these zones have stretching boundaries, it is only fortuitous that the shear direction coincides with one of the principal stretching directions of the boundaries. Therefore, most of these deformation zones are expected to follow triclinic deformation paths.

Fabrics that cannot be explained in terms of a single monoclinic deformation are common. Often they are interpreted in terms of overprinting, but some of these fabrics, such as lineations in transcurrent shear zones that vary between vertical and horizontal (e.g. Lin *et al.*, 1998), and cleavage transected folds, can also be interpreted in terms of a single triclinic deformation. Similarly, the absence of sheath folds in areas where folds have been significantly rotated, can also be due to triclinic flow.

Another example of a fabric that cannot be satisfactorily explained by monoclinic flow has been presented by Worley and Wilson (1996). They observe snowball garnets, rotated during D_2/D_3, that have a rotation axis oblique to coeval mineral lineations. They attempt to interpret the data in terms of monoclinic flow, but acknowledge the conflicting nature of the evidence. It is impossible to reconcile the three-dimensional geometry of the garnet inclusion trails with a steady monocli-

nic deformation path. The data is readily explained however, by triclinic flow. The rotation axis is parallel to the vorticity vector whereas the lineation is trying to track the $\dot{\epsilon}_c$ direction of the stretching boundary, i.e. the dip line. Thus we suggest that deformation may have followed a steady triclinic path and the zone a sinistral-reverse-thinning-zone.

It is very difficult to constrain natural deformation paths (Hudleston and Lan, 1993). Not only can triclinic flow result in monoclinic fabrics especially at large strains as mentioned above, but not all triclinic fabrics are a product of triclinic flow. They can result from oblique superposition of fabric and kinematics, both of higher symmetry. Further the initial fabric needs not be a deformation fabric (e.g. oblique interaction of a cylindrical sedimentary fabric and monoclinic flow can result in a final triclinic fabric). To establish criteria for recognizing triclinic deformation paths is difficult and unique answers are likely to be rare. However, an understanding of the characteristics of triclinic flow should lead to better interpretation of natural fabrics.

Acknowledgements—We thank Win Means and Brett Freeman for review comments, Shoufa Lin and Richard Brown for discussion. DJ particularly thanks S. Lin for getting him interested in 'oblique transpression'. This project was supported by the Natural Science and Engineering Research Council of Canada (NSERC) through a post-doctoral fellowship to DJ and a research grant to PFW.

REFERENCES

Astarita, G. (1979) Objective and generally applicable criteria for flow classification. *Journal of Non-Newtonian Fluid Mechanics* **6,** 69–76.

Bobyarchick, A. R. (1986) The eigenvalues of steady state flow in Mohr space. *Tectonophysics* **122,** 35–51.

Caron, A. and Williams, P. F. (1988) The kinematic indicators of the Love Cove Group in the northeastern Newfoundland. *Geological Association of Canada Program with Abstracts* **13,** A17.

Celma, A. G. (1982) Domainal and fabric heterogeneities in the Cap de Creus quartz mylonites. *Journal of Structural Geology* **4,** 443–455.

DeMets, C. (1992) Oblique convergence and deformation along the Kuril and Japan trenches. *Journal of Geophysical Research* **97,** 17,615–17,625.

Dutton, B. J. (1997) Finite strains in transpression zones with no boundary slip. *Journal of Structural Geology* **19,** 1189–1200.

Elliott, D. (1972) Deformation paths in structural geology. *Bulletin of the Geological Society of America* **83,** 2621–2635.

Fitch, T. J. (1972) Plate convergence, transcurrent faults, and internal deformation adjacent to Southeast Asia and the western Pacific. *Journal of Geophysical Research* **77,** 4432–4460.

Fossen, H. and Tikoff, B. (1993) The deformation matrix for simultaneous simple shearing, pure shearing and volume change, and its application to transpression–transtension tectonics. *Journal of Structural Geology* **15,** 413–422.

Frost, H. J. and Ashby, M. F. (1982) *Deformation-mechanism Maps. The Plasticity and Creep of Metals and Ceramics*. Pergamon Press, Oxford.

Gao, L. and Wallace, T. C. (1995) The 1990 Rudbar–Tarom Iranian earthquake sequence: evidence for slip partitioning. *Journal of Geophysical Research* **100,** 15,317–15,332.

Goodwin, L. B. and Williams, P. F. (1996) Deformation path partitioning within a transpressive shear zone, Marble Cove, Newfoundland. *Journal of Structural Geology* **18,** 975–990.

Hanmer, S. and Passchier, P. F. (1991) Shear-sense indicators: a review. *Geological Survey of Canada Paper* **90-17**.

Harland, W. B. (1971) Tectonic transpression in Caledonian Spitsbergen. *Geological Magazine* **108,** 27–42.

Hobbs, B. E., Means, W. D. and Williams, P. F. (1982) The relationship between foliation and strain: an experimental investigation. *Journal of Structural Geology* **4,** 411–428.

Hudleston, P. J. and Lan, L. (1993) Information from fold shapes. *Journal of Structural Geology* **15,** 253–264.

Jeffrey, A. (1995) *Handbook of Mathematical Formulas and Integrals*. Academic Press, New York.

Jiang, D. (1994a) Vorticity determination, distribution, partitioning and the heterogeneity and non-steadiness of natural deformations. *Journal of Structural Geology* **16,** 121–130.

Jiang, D. (1994b) Flow variation in layered rocks subjected to bulk flow of various kinematic vorticities: theory and geological implications. *Journal of Structural Geology* **16,** 1159–1172.

Jiang, D. (1996) Kinematics and mechanisms of rock deformation, with reference to the East Athabasca mylonite Triangle, Saskatchewan, Canada. Unpublished PhD thesis. University of New Brunswick, Fredericton, Canada.

Jiang, D. and White, J. C. (1995) Kinematics of rock flow and the interpretation of geological structures, with particular reference to shear zones. *Journal of Structural Geology* **17,** 1249–1265.

Jones, R. R., Holdsworth, R. E. and Baily, W. (1997) Lateral extrusion in transpression zones. *Journal of Structural Geology* **19,** 1201–1217.

Jones, R. R. and Tanner, P. W. G. (1995) Strain partitioning in transpression zones. *Journal of Structural Geology* **17,** 793–802.

Krantz, R. W. (1995) The transpressional strain model applied to strike-slip, oblique-convergent and oblique-divergent deformation. *Journal of Structural Geology* **17,** 1125–1137.

Lin, S. (1992) The stratigraphy and structural geology of the southeastern Cape Breton Highlands National Park and its implications for the tectonic evolution of Cape Breton Island, Nova Scotia, with emphasis on lineations in shear zones. Unpublished Ph.D thesis. University of New Brunswick, Fredericton, Canada.

Lin, S., Jiang, D. and Williams, P. F. (1998) Transpression (or–transtension) zones of triclinic symmetry: natural example and theoretical modelling. In *Continental Transpressional and Transtensional Tectonics*, eds R. E. Holdsworth, R. Strachan and J. Dewey, pp. 41–57. Geological Society, London, Special Publication, **135**.

Lin, S. and Williams, P. F. (1992) The origin of ridge-in-groove slickenside striae and associated steps in an *S–C* mylonite. *Journal of Structural Geology* **14,** 315–321.

Lister, G. S. and Williams, P. F. (1979) Fabric development in shear zones: theoretical controls and observed phenomena. *Journal of Structural Geology* **1,** 283–297.

Lister, G. S. and Williams, P. F. (1983) The partitioning of deformation in flowing rock masses. *Tectonophysics* **92,** 1–33.

Liu, X., McNally, K. C. and Shen, Z.-K. (1995) Evidence for a role of the downgoing slab in earthquake slip partitioning at oblique subduction zones. *Journal of Geophysical Research* **100,** 15,351–15,372.

McCaffrey, R. (1992) Oblique plate convergence, slip vectors, and forearc deformation. *Journal of Geophysical Research* **97,** 8905–8915.

McKenzie, D. (1979) Finite deformation during fluid flow. *Geophysical Journal of Royal Astrolomical Society* **58,** 689–715.

Means, W. D. (1981) The concept of steady-state foliation. *Tectonophysics* **78,** 179–199.

Means, W. D. (1987) A newly recognized type of slickenside striation. *Journal of Structural Geology* **9,** 585–590.

Means, W. D. (1995) Shear zones and rock history. *Tectonophysics* **247,** 157–160.

Means, W. D., Hobbs, B. E., Lister, G. S. and Williams, P. F. (1980) Vorticity and non-coaxiality in progressive deformations. *Journal of Structural Geology* **2,** 371–378.

Mitra, G. (1978) Ductile deformation zones and mylonites: the mechanical processes involved in the deformation of crystalline basement rocks. *American Journal of Science* **278,** 1057–1084.

Nadai, A. (1963) *Theory of Flow and Fracture of Solids*. McGraw-Hill, New York.

Passchier, C. W. (1988) The use of Mohr circles to describe non-coaxial progressive deformation. *Tectonophysics* **149,** 323–338.

Passchier, C. W. (1990) Reconstruction of deformation and flow parameters from deformed vein sets. *Tectonophysics* **180,** 185–199.

Passchier, C. W. (1991) The classification of dilatant flow types. *Journal of Structural Geology* **13,** 101–104.

Passchier, C. W. (1997) The fabric attractor. *Journal of Structural Geology* **19,** 113–127.

Passchier, C. W. (1998) Monodinic model shear zones. *Journal of Structural Geology*. **20,** 1121–1137.

Passchier, C. W. and Trouw, R. A. J. (1996) *Microtectonics*. Springer-Verlag, New York.

Platt, J. P. and Behrmann, J. H. (1986) Structures and fabrics in a crustal scale shear zone, Betic Cordillera, SE Spain. *Journal of Structural Geology* **8,** 15–33.

Ramberg, H. (1975) Particle paths, displacement and progressive strain applicable to rocks. *Tectonophysics* **28,** 1–37.

Ramsay, J. G. (1980) Shear zone geometry: a review. *Journal of Structural Geology* **2,** 83–89.

Ramsay, J. G. and Graham, R. H. (1970) Strain variation in shear belts. *Canadian Journal of Earth Sciences* **7,** 786–813.

Ranalli, G. (1987) *Rheology of the Earth*. Allen and Unwin, Boston.

Robin, P.-Y. F. and Cruden, A. R. (1994) Strain and vorticity patterns in ideally ductile transpressional zones. *Journal of Structural Geology* **16,** 447–466.

Sanderson, D. J. and Marchini, W. R. D. (1984) Transpression. *Journal of Structural Geology* **6,** 449–458.

Shen-Tu, B., Holt, W. E. and Haines, A. J. (1995) Intraplate deformation in the Japanese Islands: a kinematic study of intraplate deformation at a convergent plate margin. *Journal of Geophysical Research* **100,** 24,275–24,293.

Simpson, C. and De Paor, D. G. (1993) Strain and kinematic analysis in general shear zones. *Journal of Structural Geology* **15,** 1–20.

Teyssier, C. B., Tikoff, B. and Markley, M. (1995) Oblique plate motion and continental tectonics. *Geology* **23,** 447–450.

Tikoff, B. and Teyssier, C. (1994) Strain modeling of displacement-field partitioning in transpressional orogens. *Journal of Structural Geology* **16,** 1575–1588.

Treagus, S. H. (1983) A theory of finite strain variation through contrasting layers, and its bearing on cleavage refraction. *Journal of Structural Geology* **5,** 351–368.

Truesdell, C. A. (1953) Two measures of vorticity. *Journal of Rational Mechanics Analysis* **2,** 173–217.

Truesdell, C. A. and Toupin, R. A. (1960) The classic field theory. In *Encyclopedia of Physics*. *Volume II: Principles of classical mechanics and field theory*, ed. S. Flügge, pp. 226–793. Springer-Verlag, Berlin.

White, N. (1994) An inverse method for determining lithospheric strain rate variation on geological time scales. *Earth and Planetary Science Letters* **122,** 351–371.

Williams, P. F. (1976) Relationships between axial-plane foliations and strain. *Tectonophysics* **30,** 181–196.

Williams, P. F., Means, W. D. and Hobbs, B. E. (1977) Development of axial-plane slaty cleavage and schistosity in experimental and natural materials. *Tectonophysics* **42,** 139–158.

Williams, P. F. and Schoneveld, C. (1981) Garnet rotation and the development of axial plane crenulation cleavage. *Tectonophysics* **78,** 307–334.

Williams, P. F. and Vernon, R. H. (in press) Origin of a vertical lineation in transcurrent conjugate shear zones at Broken Hill, Australia. *Tectonophysics*.

Worley, B. A. and Wilson, C. J. L. (1996) Deformation partitioning and foliation reactivation during transpressional orogenesis, an example from the Central Longmen Shan, China. *Journal of Structural Geology* **18,** 395–411.